

Characterizing the Conformational Ensemble of Monomeric Polyglutamine

Xiaoling Wang,^{1,3} Andreas Vitalis,^{2,3} Matthew A. Wyczalkowski,^{1,3} and Rohit V. Pappu^{1,3*}

¹Department of Biomedical Engineering, Washington University, St. Louis, Missouri

²Molecular Biophysics Program, Division of Biology and Biomedical Sciences, Washington University, St. Louis, Missouri

³Center for Computational Biology, Washington University, St. Louis, Missouri

ABSTRACT Studies of synthetic polyglutamine peptides *in vitro* have established that polyglutamine peptides aggregate via a classic nucleation and growth mechanism. Chen and colleagues [Proc Natl Acad Sci U S A 2002;99:11884–11889] have found that monomeric polyglutamine, which is a disordered statistical coil in solution, is the critical nucleus for aggregation. Therefore, nucleation of β -sheet-rich aggregates requires an initial disorder to order transition, which is a highly unfavorable thermodynamic reaction. The questions of interest to us are as follows: What are the statistical fluctuations that drive β -sheet formation in monomeric polyglutamine? How do these fluctuations vary with chain length? And why is this process thermodynamically unfavorable, that is, why is monomeric polyglutamine disordered? To answer these questions we use multiple molecular dynamics simulations to provide quantitative characterization of conformational ensembles for two short polyglutamine peptides. We find that the ensemble for polyglutamine is indeed disordered. However, the disorder is inherently different from that of denatured proteins and the average compactness and magnitude of conformational fluctuations increase with chain length. Most importantly, the effective concentration of sidechain primary amides around backbone units is inherently high and peptide units are solvated either by hydrogen bonds to sidechains or surrounding water molecules. Due to the multiplicity of backbone solvation modes the probability associated with any specific backbone conformation is small, resulting in a conformational entropy bottleneck which makes β -sheet formation in monomeric polyglutamine thermodynamically unfavorable. *Proteins* 2006;63:297–311. © 2005 Wiley-Liss, Inc.

Key words: polyglutamine; disorder; nucleation; aggregation; β -sheet; order parameter

INTRODUCTION

Huntington's disease is a genetic disorder that is linked to mutations that lead to polyglutamine expansions in the N-terminal region of the protein huntingtin.² There is a strong correlation between the age of onset in Huntington's disease and the length of polyglutamine expansions coded for by exon 1 of huntingtin.^{3,4} Disease penetrance is especially aggressive when the number of consecutive

glutamine residues crosses the 35- to 40-residue threshold.² Polyglutamine expansions in proteins other than huntingtin are associated with eight other disorders including spinal and bulbar muscular atrophy, dentatorubral-pallidoluysian atrophy, and six spinocerebellar ataxias.^{5,6}

Neuropathology studies have shown that expanded polyglutamine tracts self-associate to form ordered protein aggregates.^{7–9} Aggregates appear to be rich in β -sheets and low-resolution structural studies indicate the cross- β architecture that is associated with amyloid superstructures.^{10–12} Postmortem examinations of Huntington's disease patients show that aggregates are deposited as intranuclear inclusions within neurons.^{8,9} Uptake of polyglutamine aggregates into the nucleus has been linked to cell death in cell culture studies.¹³

Why are expanded polyglutamine tracts prone to aggregation? The biophysical principles that underlie protein aggregation have been the subject of intense studies over the past 5 years.^{14–26} Dobson and coworkers have shown that the propensity to aggregate is a generic attribute of polypeptide chains, especially of main-chain atoms that are common to all protein sequences.^{21,23} It is reasonable to assume that the strong tendency of polyglutamine tracts to aggregate may be attributed to the duplication of backbone-like polar moieties in the sidechains.^{2,10,41}

Dobson and coworkers have also shown that aggregation propensities of polypeptides can be closely related to the hydrophobicity of amino acid sequences.^{27,28} The more hydrophobic a sequence, the more readily it aggregates. Polyglutamine is a polar molecule and its propensity to aggregate is an interesting outlier in that it does not appear to come under the purview of recent predictive models.^{27,28}

The process of aggregation has also been the subject of considerably scrutiny. There is growing evidence that intermediates accessible along pathways to amyloid are just as toxic — if not more toxic — than amyloids.^{29–34} In

Contract grant sponsor: March of Dimes Foundation; Contract grant sponsor: National Science Foundation

*Correspondence to: Rohit Pappu, Department of Biomedical Engineering, Center for Computational Biology, Washington University in St. Louis, Campus Box 1097, St. Louis, MO 63130. E-mail: pappu@biomed.wustl.edu

Received 5 August 2005; Revised 22 August 2005; Accepted 23 August 2005

Published online 18 November 2005 in Wiley InterScience (www.interscience.wiley.com). DOI: 10.1002/prot.20761

most systems, amyloid formation appears to be a consequence of the self-association of either denatured proteins or natively unfolded polypeptides.²⁵ Further evidence for unfoldedness being an important trigger for peptide insolubility or aggregation comes from work in the Mütter group.^{35,36} Sequences that are prone to be unfolded are termed difficult sequences^{35,36} for peptide synthesis because the overall yields drop dramatically with peptide length. The drop in yield is a direct consequence of peptide aggregation. The main message from these studies is that peptides that prefer to be statistical coils are also likely to aggregate readily.³⁶

In vitro studies of recombinant proteins^{37–40} with polyglutamine expansions and synthetic polyglutamine peptides^{1,26,41–44} of varying lengths recapitulate many of the aggregation related phenotypes associated with proteins linked to disease. These include the sharp length-dependent propensity to form aggregates,^{1,26,37,38,43} the ability to recruit short polyglutamine peptides into growing aggregates,⁴³ the formation of aggregates with amyloid-like superstructure,¹² and the formation of spherical and annular oligomers.⁴⁰

Wetzel and coworkers have studied length-dependent aggregation of synthetic polyglutamine peptides.²⁶ Aggregation requires high peptide concentrations (ca. 10 μM) and kinetic data are consistent with classic nucleation-growth behavior.^{1,12,26,43,44} Lag times and critical concentrations decrease with increasing chain length.^{1,12,43} Analysis of kinetic data for aggregation of peptides of different lengths leads to the conclusion that the monomer — a single polyglutamine chain — is the critical nucleus for aggregation.^{1,26} Following upon this observation, Wetzel and coworkers proposed a model where the nucleus is assumed to be in a rapid pre-equilibrium with the bulk phase monomer.¹

Irrespective of peptide length, monomeric polyglutamine is unfolded in aqueous buffers. This fact is established by data from CD spectroscopy.^{1,12,39,41,42,45} Therefore, nucleation which is a disorder to order transition is akin to highly unfavorable folding (thermodynamic) reaction.¹ The proposed pre-equilibrium between bulk phase monomer and the nucleus for aggregation is written as:

$\text{M}_b \xrightleftharpoons[k_{-1}]{k_1} \text{M}_{N^*}$, where M_b denotes bulk phase monomer, M_{N^*} denotes the nucleus, and the pre-equilibrium constant $K_{N^*} = \frac{k_1}{k_{-1}}$ is defined as the ratio of the rates for the forward and reverse reactions, k_1 and k_{-1} , respectively. By definition the nucleus is populated with very low probability and K_{N^*} is expected to be very small for short and long chains. The length-dependent increase in aggregation is associated with a length-dependent increase in K_{N^*} , although this parameter will overwhelmingly favor the bulk phase monomer.¹

Why is K_{N^*} small? In other words, why does polyglutamine prefer to be disordered in solution? And what is the mechanism by which polyglutamine peptides transiently populate intramolecular β -sheets that can elongate to form amyloid fibers? To answer these questions, we have

begun a series of studies to characterize the conformational ensembles of polyglutamine peptides of different chain lengths.

Aggregation in vitro requires concentrations in the micromolar range. Why then is it important to study the ensemble of monomeric polyglutamine? The monomeric ensemble contributes to nucleation of aggregation in three ways: (1) through the stability of the nucleus quantified by K_{N^*} ; (2) through the thermodynamic driving force⁴⁷ for aggregation $\Delta\mu$ which is written as $\Delta\mu = \frac{G_A - G_M}{n}$, where G_A and G_M are free energies for the aggregate and monomer and n is the number of polyglutamine molecules; and (3) through the work for nucleating a cluster⁴⁷ written as $W = -\Delta\mu + G_{\text{ex}}$. Here, G_{ex} is the so-called cluster excess free energy and corresponds to the free energy penalty associated with creating a phase boundary.

Molecular simulations provide detailed atomistic information regarding conformational ensembles. Such information is inaccessible to conventional spectroscopic probes, which are used to probe disordered ensembles. Decreasing CPU costs combined with major improvements in sampling algorithms^{48–52} have spurred the use of molecular simulations for a range of mechanistic studies of protein folding^{51–56} and aggregation phenomena.^{57–61} Especially important are insights drawn from simulations regarding the unfolded states of proteins and peptides.^{62–68}

Here, we use multiple molecular dynamics simulations to provide quantitative characterization of the conformational ensembles for two polyglutamine peptides with 5 and 15 residues, respectively. Our data provide a plausible explanation for the source of disorder in monomeric polyglutamine. This in turn leads to a reasonable hypothesis for why β -sheet formation is unfavorable for polyglutamine. We first discuss the methodology used in our calculations. This is followed by a presentation of the results and a discussion of implications for the questions of interest.

METHODS

We report results from our analysis of multiple molecular dynamics simulations for two polyglutamine peptides. The peptides studied are: *N*-acetyl-(Gln)₅-*N'*-methylamide and *N*-acetyl-(Gln)₁₅-*N'*-methylamide. The N- and C-termini in both peptides are capped with blocking groups to avoid complications due to charged termini. To be concise we refer to the peptide with 5 glutamine residues as Q5 and the peptide with 15 glutamine residues as Q15.

Force Field

Parameters from the all atom OPLS-AA force field^{69,70} were used for the peptides. The four-site TIP4P model⁷¹ was used to model water molecules. The TIP4P model is one of several water models in the TIPxP series.⁷¹ It is an improvement over the popular three-site TIP3P model, especially in its ability to reproduce structural and thermodynamic properties of bulk water. One advantage of using the OPLS-AA force field is that it allows flexibility in the choice of water models. This option is unavailable in simulations with other nonpolarizable force fields.

The Simulation Engine

All molecular dynamics simulations were performed using the GROMACS package.^{72,73} The isothermal-isobaric (NPT) ensemble was used in all equilibration and production runs. The equilibrium temperature and pressure for all molecular dynamics simulations was $T = 298$ K and $P = 1$ bar, respectively. Temperature and pressure were controlled using the weak-coupling algorithms of Berendsen and coworkers.⁷⁴ The control parameters are $\tau = 0.2$ ps for the thermostat and $\kappa = 4.5 \times 10^{-5} \text{bar}^{-1}$ for the compressibility. A 2.0 fs time step was used in all of our simulations. All bond lengths were constrained using the LINCS algorithm.⁷⁵ Neighbor lists for nonbonded interactions were updated every 10 time steps.

In each of the molecular dynamics simulations, a starting conformation (see below) for the peptide of interest (Q5 or Q15) was chosen with the peptide placed at the center of a dodecahedral box of pre-equilibrated water molecules. Dimensions of the central box are different for the two peptides. For Q5 and Q15, the central simulation box is such that the shortest distance between opposing faces of the polyhedron are 40 Å and 45 Å with 1400 and 1900 water molecules, respectively. The box sizes are chosen to ensure that when peptides adopt realistic extended conformations — as determined by the distribution of conformations generated in the excluded volume limit (see below) — at least eight layers of water molecules separate the molecules in the central cell from their images.

Periodic boundary conditions with the minimum image convention were applied to ensure the absence of macroscopic interfaces. At the beginning of each simulation, a short 0.4 ps simulation of the peptide + water system in the NVT (isothermal-isochoric) ensemble was used to relieve any steric overlaps between peptide atoms and between the peptide and surrounding water molecules. Additional 50 ps (for Q5) and 100 ps simulations (for Q15) in the NPT ensemble were used as initial equilibration runs. The end points of these simulations were the starting points for 15 ns production runs.

Conformational ensembles were constructed by analyzing 60 independent 15 ns simulations for the Q5 peptide and 90 independent 15 ns simulations for the Q15 peptide. The cumulative simulation times are 0.9 μs and 1.35 μs for Q5 and Q15, respectively. In each simulation, snapshots of peptide conformations are written out in 0.8 ps intervals for Q5 and 2 ps intervals for Q15.

Long-Range Interactions

A 10 Å spherical cutoff with truncation was used for the van der Waals and Coulomb interactions. The choice of spherical cutoffs requires some justification because it is well known that long-range interactions have a significant influence on simulation results.^{76,77} We have previously quantified the effects of long-range interactions in molecular dynamics simulations using two different methods for evaluating Coulomb interactions — spherical cutoffs and Ewald sums.⁷⁸ Free energy surfaces for peptides that are net electro-neutral are not sensitive to the algorithm used

to handle long-range electrostatics so long as the cutoff distance is not too short (Pappu, unpublished data). In simulations of peptides that do not have a net charge, the solute can be viewed as a concatenation of electro-neutral groups. Similarly, water molecules are also electro-neutral. Over large separations electrostatic interactions reduce to dipole-dipole interactions which are convergent and decay more rapidly than charge-charge interactions. The main conclusion is as follows: For the particular problem of capped polyglutamine peptides in water, spherical cutoffs can be used instead of Ewald sums without introducing significant errors. Similar conclusions have been reported in the literature for other electro-neutral peptides and polymers in water and aqueous mixtures.⁷⁹

Quantifying Conformational Ensembles Using Probability Distribution Functions

Our goal is to quantify the equilibrium ensemble for monomeric polyglutamine as a function of chain length. This is accomplished by constructing probability distribution functions (PDFs), one each for Q5 and Q15. We denote a PDF as $\rho(a,b)$, $0 \leq \rho \leq 1$, where a and b are two conformation-specific, preferably independent, order parameters.

The choice of order parameters is not trivial and this topic has received considerable attention in formulations of molecular simulations^{51,80–82} and energy landscape theories.⁸³ The first order parameter is invariably the radius of gyration (R_g) which quantifies the size of a polypeptide. The second parameter helps quantify the shape, conformation, or topology of the molecule. When the native conformation is known, several options exist for the second order parameter which quantifies overall shape or conformation.^{82,83} The choice is governed by whether one is interested in extracting information regarding transition states (kinetics) or conformational equilibria (thermodynamics).

For polyglutamine in water, we have no a priori knowledge of the preferred shape or conformation. Therefore, we adapt ideas from polymer physics to select two order parameters.⁸⁴ We use R_g to quantify the sizes of peptides and asphericity (δ)⁸⁴ to quantify overall shape. Both R_g and δ are measurable using scattering experiments.^{84,86} If the value of R_g is small, the conformation is compact and if R_g is large the conformation is swollen or expanded.

Asphericity is a dimensionless quantity and for a given conformation it is defined as: $\delta = 1 - 3 \frac{L_1^2 L_2^2 + L_2^2 L_3^2 + L_3^2 L_1^2}{(L_1^2 + L_2^2 + L_3^2)^2}$ and $0 \leq \delta \leq 1$. L_i ($i = 1, 2, 3$) are the eigenvalues of the radius of gyration tensor.⁸⁵ $\delta \approx 1$ for a rodlike polymer and $\delta \approx 0$ for a perfect sphere. Oblate spheroids, prolate spheroids, and ellipsoids have asphericity values that are greater than 0.2 and less than 0.7.⁸⁴ If δ is small, the chain assumes a roughly spherical shape and is globular. For intermediate values, $0.3 \leq \delta \leq 0.5$, the chain is a loosely packed globule.⁸⁴

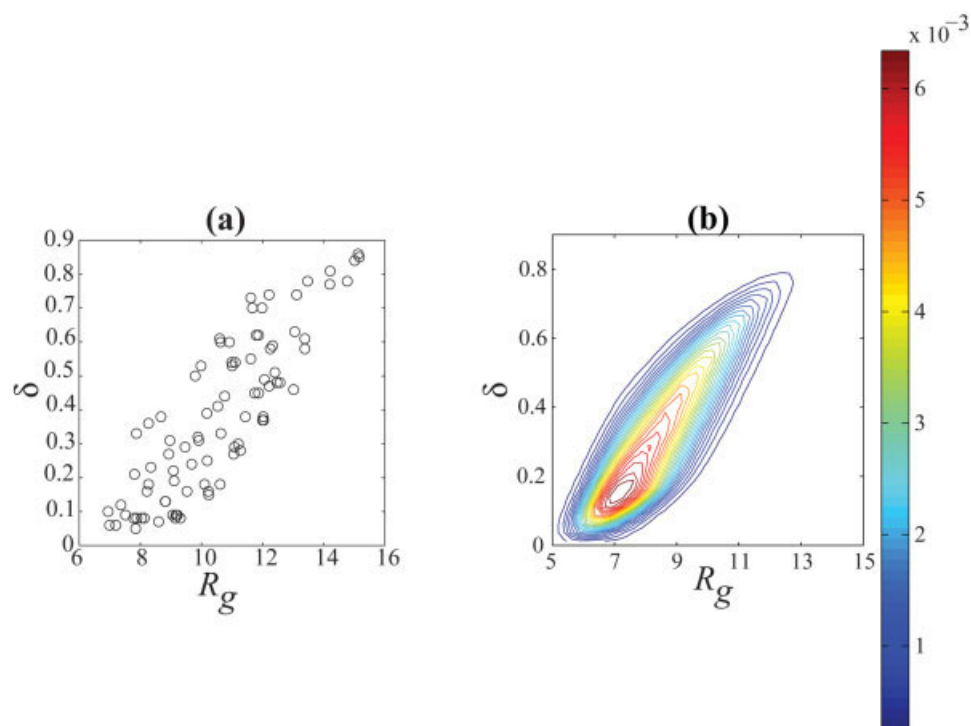


Figure 1.

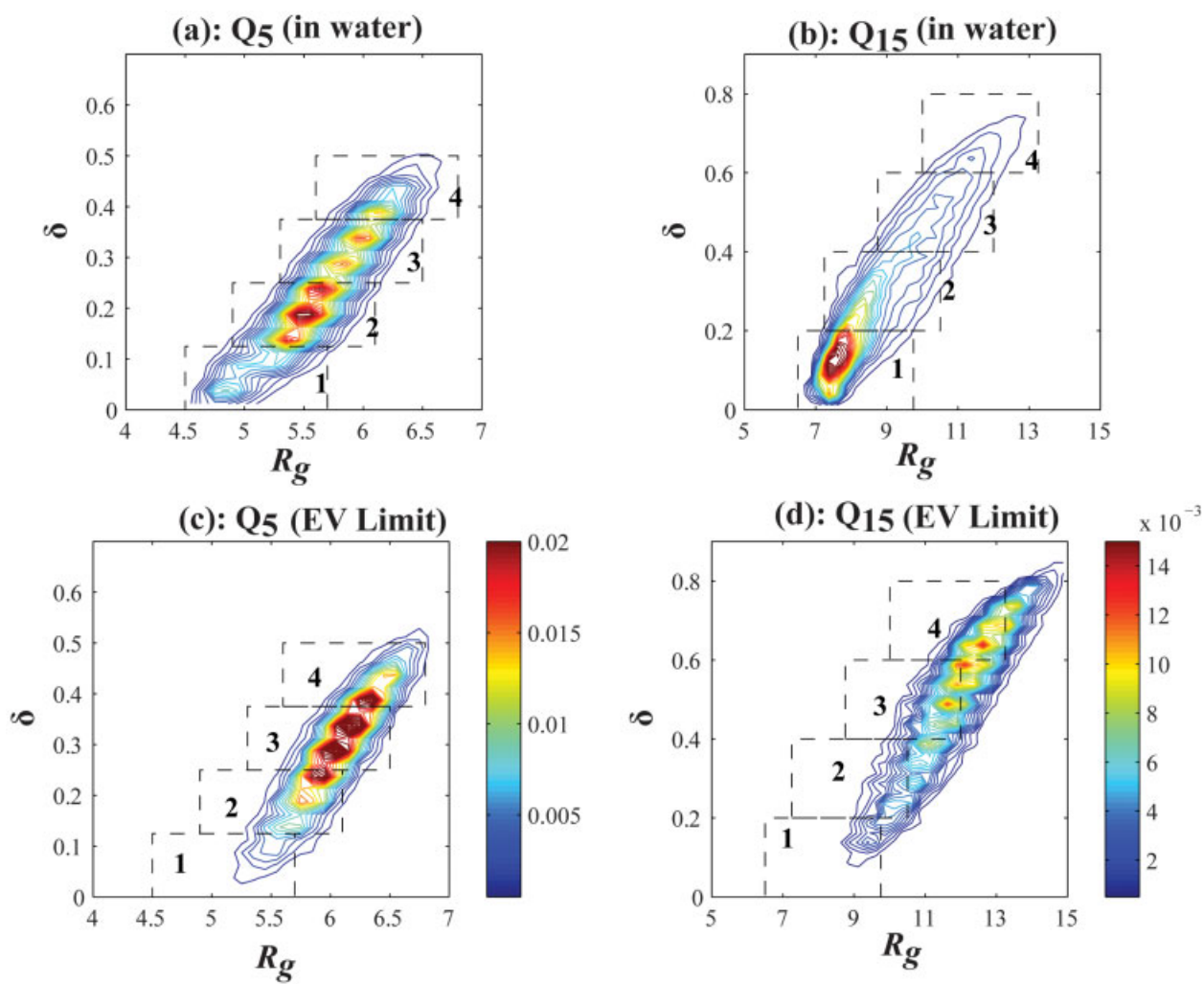


Figure 3.

Algorithm to Construct the PDF $\rho(\delta, R_g)$

We use a bootstrapping method⁹¹ to stitch together information from multiple, unbiased trajectories in order to construct an estimate for $\rho(\delta, R_g)$.

1. Setting up initial conformations: We used a Metropolis Monte Carlo (MMC) algorithm⁸⁷ to sample conformational space for each peptide. Details regarding the MMC simulations are described elsewhere.⁶⁸ The potential functions we use are such that conformations in the ensemble generated using the MMC simulations are self-avoiding and uniformly adopt all realizable values in (δ, R_g) space. Representative conformations corresponding to different values of δ and R_g are randomly drawn from the initial ensemble. These conformations represent the starting geometries for independent molecular dynamics simulations. Figure 1(a) shows the order parameters of the initial conformations for the 90 molecular dynamics simulations of Q15.

To emphasize that these initial (δ, R_g) values span all of conceivable space, Figure 1(b) shows the PDF $\rho_{id}(\delta, R_g)$ for an ideal Q15 peptide.⁸⁸ To generate $\rho_{id}(\delta, R_g)$, we freeze all bond lengths and bond angles at equilibrium values⁸⁹ and constrain the peptide units to be planar and trans. We then turn off all other interatomic interactions and generate an ensemble of conformations via a Monte Carlo procedure that randomly varies the backbone (ϕ, ψ) and sidechain χ -angles. Figure 1(b) illustrates that constraints of chain connectivity naturally give rise to an oblong shape for the two-dimensional PDFs. Comparison of Figures 1(a,b) establishes that (δ, R_g) values of initial conformations for the different dynamics simulations uniformly cover the realizable order parameter space.

2. Collecting data for construction of $\rho(\delta, R_g)$: In each of the 60 simulations for Q5 and 90 simulations for Q15 we discard the first 3 ns of data. This was based on the observation that in a typical molecular dynamics simulation, for both Q5 and Q15, the characteristic decay time for the autocorrelation function⁹⁰ of R_g was approximately 3 ns. Pruned data were used in subsequent analysis.
3. Bootstrap procedure for constructing $\rho(\delta, R_g)$:

- (a) To analyze the last 12 ns of each molecular dynamics trajectory a sampling frequency τ_s is chosen at random from the interval $4 \text{ ps} \leq \tau_s \leq 40 \text{ ps}$. N_s distinct snapshots are selected from the trajectory in intervals of τ_s ps such that $N_s \tau_s = 12 \text{ ns}$.
- (b) Step (a) is repeated for each independent trajectory of the peptide of interest and the data are pooled.
- (c) The pooled data are used to construct a two-dimensional histogram in the two-dimensional order parameter space. The number of points (N_s) sampled from each trajectory and the total numbers of trajectories are used to normalize the histogram.
- (d) Steps (a)–(c) are repeated 50 times. This is analogous to the technique of bootstrapping with replacement.⁹¹ The different normalized histograms are averaged to construct the desired PDF, $\rho(\delta, R_g)$. The standard deviation is an estimate of the error in our construction of $\rho(\delta, R_g)$.

Our strategy is similar to the ensemble dynamics methodology of Pande and coworkers.⁵⁰ The only difference is in the use of different starting conformations for each simulation. The bootstrapping procedure for constructing $\rho(\delta, R_g)$ is valid only if each trajectory is not confined to a small region around its starting point in (δ, R_g) -space.⁹² The general validity of our procedure is established in Figure 2. Here, we show the typical span in order parameter space for representative 15 ns trajectories of the Q5 and Q15 peptides, respectively. It is clear that the trajectories are not confined to a specific region and that the full range of realizable space can be sampled.

RESULTS

$\rho(\delta, R_g)$ for Q5 and Q15

PDFs for the Q5 and Q15 peptides in water are shown in Figures 3(a,b). We tabulate cumulative statistics for different regions of the order parameter space by superposing ad hoc rectangular boxes on the contours shown in Figures 3(a,b). The box sizes are chosen to maximize overlap across the oblong contour map and cover a range of δ and R_g values within each box. Dimensions for the ad hoc boxes are different for Q5 and Q15. Table I also shows cumulative statistics for each of the four regions identified for Q5 and Q15. Cumulative statistics for a given box are computed by integration over ρ in that box.

The statistics shown in Table I lead to the following observations: If the peptides were structured one would expect the cumulative statistics for at least one of the ad hoc boxes to be dominant. We make this assertion based on the range of δ and R_g values for each ad hoc box. Figures 3(a,b), as well as data in Table I, emphasize that this is not the case. The ensembles of Q5 and Q15 are clearly disordered in that the peptides do not have an overwhelming preference for specific regions of the order parameter space. There is a length dependence to this disorder in that there is a marked preference for compact, globular conformations in the Q15 ensemble. The Q5 peptide is too short to realize such preferences.

Our conclusion that polyglutamine ensemble is disordered is consistent with the findings of Chen and col-

Fig. 1. (a): (δ, R_g) values of initial conformations for the 90 molecular dynamics simulations of Q15. (b): Illustration of calculated $\rho_{id}(\delta, R_g)$ for an ideal 15-mer of polyglutamine. This illustrates the generality of the oblong shape of the two-dimensional PDFs for polypeptide chains.

Fig. 3. (a): $\rho(\delta, R_g)$ from the bootstrap analysis of molecular dynamics simulations for Q5. Ad hoc rectangular envelopes are superimposed on the PDF to compute cumulative statistics. Numerical labels, 1 to 4, are assigned to each region. (b): $\rho(\delta, R_g)$ from the bootstrap analysis of molecular dynamics simulations for Q15. Numerical labels, 1 to 4, are assigned to each region superimposed on the PDF. (c): Contour maps of $\rho_{EV}(\delta, R_g)$ for Q5. The boxes superposed on this PDF are identical to the ones used in Figure 3(a). (d): Contour maps of $\rho_{EV}(\delta, R_g)$ for Q15. The boxes superposed on this PDF are identical to the ones used in Figure 3(b). Dimensions of ad hoc boxes and cumulative statistics for all four PDFs are shown in Table I. Figures 3(a,c) share the same color bar. This is located adjacent to Figure 3(c). The color bar for the Q15 PDFs is located to the right of Figure 3(d).

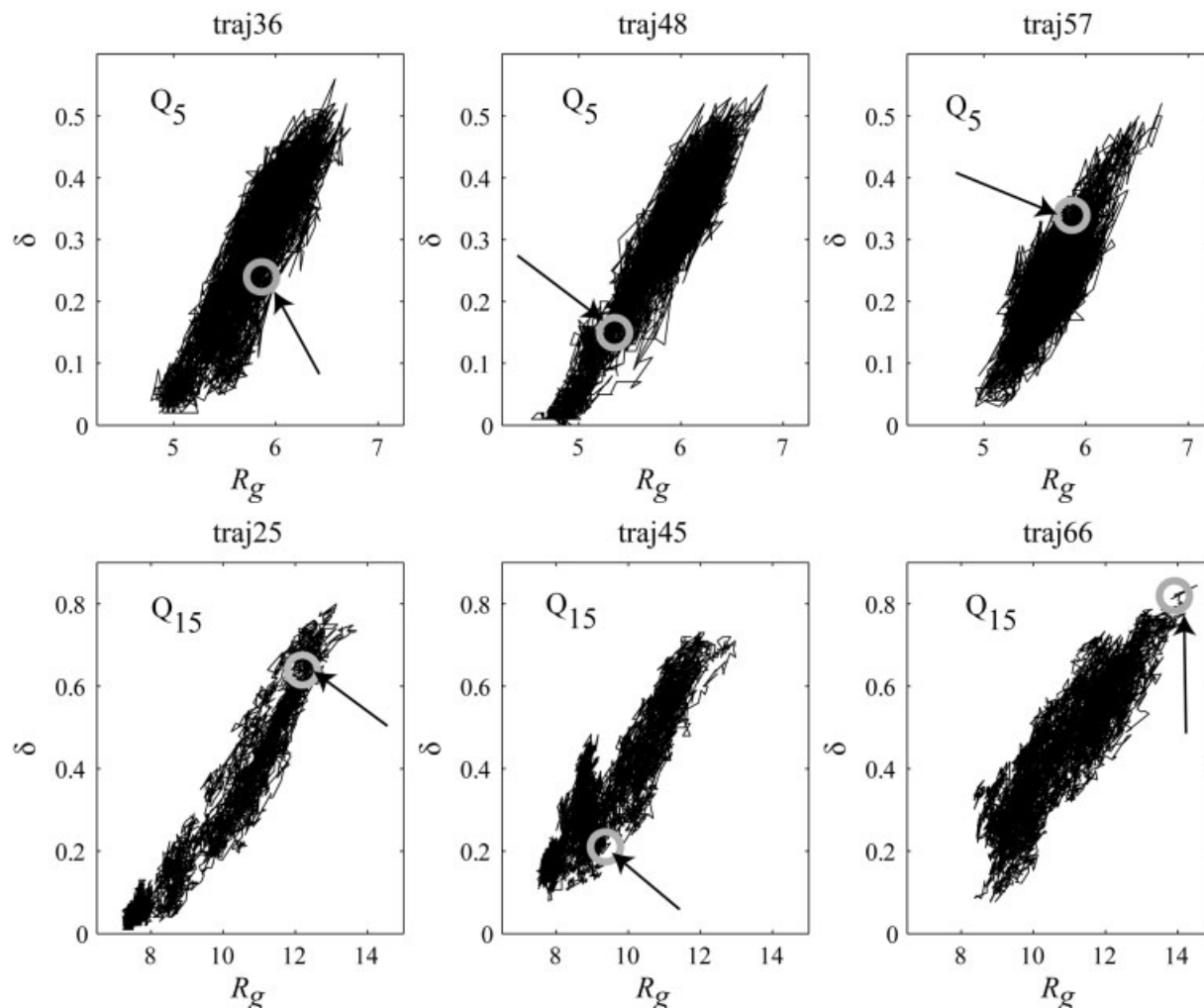


Fig. 2. Span of sample trajectories. Top row shows a mapping of (δ, R_g) from three sample molecular dynamics trajectories for Q5. Bottom row shows similar information for Q15. Arrows point to (δ, R_g) values of initial conformations for each trajectory. These are also marked by gray open circles.

leagues⁴³ who used UV-CD spectroscopy to characterize the ensemble for monomeric polyglutamine. Chen and colleagues found that the CD spectra for Q5, Q15, Q28, and Q40 are roughly equivalent to each other. It is also true that the CD spectra of Chen and colleagues bear close resemblance to CD spectra for chemically denatured proteins.⁹³ The insensitivity of CD data to changes in chain length and the similarity in CD profiles to those seen for denatured proteins (especially in terms of the negative molar ellipticities in the 200 nm range) raises an interesting question.

Comparing Different Flavors of Disorder

Is the disorder seen in our simulations for polyglutamine in water akin to the disorder seen for denatured proteins? In other words, is a PDF in water similar to a PDF in denaturant and is there essentially only one type of statistical-coil state? To answer this question it would be useful to predict the PDF for polyglutamine in a denaturing environment and compare it to the PDFs shown in

Figures 3(a,b). We can do this using a recently developed model⁶⁸ that provides an accurate facsimile of the ensemble of conformations accessible to polypeptides in harshly denaturing environments such as 8M urea.⁹⁴ Such ensembles can be mimicked by simulating conformational ensembles in the excluded volume (EV) limit.^{68,86} This is because denatured polypeptides behave like polymers in a so-called good solvent and the EV limit provides an ideal mimic of good solvent conditions.

We generated conformational ensembles for Q5 and Q15 in the EV limit and used these ensembles to compute $\rho_{EV}(\delta, R_g)$. The results are shown in Figures 3(c,d). Additionally, in Figure 4 we plot the probability distributions $p\left(\frac{R_g}{\sqrt{N}}\right)$ for both Q5 and Q15 versus $\frac{R_g}{\sqrt{N}}$ because the variation of R_g with chain length N obeys well-defined scaling laws. Data are shown for the peptides in water and in the EV limit.

The conformational ensemble in water, although disordered, is inherently different from the disorder one would

TABLE I. Cumulative Statistics (%) for Each of the Four Regions Identified for Q5 and Q15*

| | Box 1 (%) | Box 2 (%) | Box 3 (%) | Box 4 (%) | Total (%) |
|-----------------|----------------|----------------|----------------|----------------|----------------|
| Q5 in water | 16.1 \pm 1.3 | 40.4 \pm 1.1 | 29.1 \pm 0.9 | 13.8 \pm 0.8 | 99.4 \pm 0.1 |
| Q5 in EV limit | 5.5 \pm 0.9 | 27.6 \pm 1.7 | 42.0 \pm 1.6 | 22.1 \pm 1.8 | 97.2 \pm 0.4 |
| Q15 in water | 36.1 \pm 3.4 | 33.1 \pm 2.0 | 22.1 \pm 1.8 | 6.7 \pm 1.0 | 98.1 \pm 0.3 |
| Q15 in EV limit | 3.0 \pm 0.5 | 8.1 \pm 0.9 | 23.6 \pm 1.3 | 21.3 \pm 0.8 | 56.1 \pm 1.5 |

*All errors are standard errors obtained from the bootstrap analysis. Column 6 shows the sum of the cumulative statistics in the four regions for each class of simulation. Sizes of ad hoc boxes in Figure 3 are as follows: 1.2 Å along R_g and 0.125 along δ for Q5, and 3.25 Å along R_g and 0.2 along δ for Q15. Definitions of the four regions for Q5 are as follows: Box 1: $4.5 \leq R_g < 5.7$ and $0 \leq \delta < 0.125$; Box 2: $4.9 \leq R_g < 6.1$ and $0.125 \leq \delta < 0.25$; Box 3: $5.3 \leq R_g < 6.5$ and $0.25 \leq \delta < 0.375$; Box 4: $5.6 \leq R_g < 6.8$ and $0.375 \leq \delta < 0.5$. Definitions of the four regions for Q15 are: Box 1: $6.5 \leq R_g < 9.75$ and $0 \leq \delta < 0.2$; Box 2: $7.25 \leq R_g < 10.5$ and $0.2 \leq \delta < 0.4$; Box 3: $8.75 \leq R_g < 12$ and $0.4 \leq \delta < 0.6$; Box 4: $10 \leq R_g < 13.25$ and $0.6 \leq \delta < 0.8$.

expect for a chain in the EV limit. In the latter case, conformations that are relatively extended with larger values of δ are favored. These differences are tabulated in Table I which provides a summary of cumulative statistics over boxes used to analyze $\rho(\delta, R_g)$ for the peptides in water. As shown in Table I, differences between $\rho(\delta, R_g)$ and $\rho_{EV}(\delta, R_g)$ increase with increasing chain length. However, in water and in the EV limit there is an increase in conformational heterogeneity as chain length increases. This is characterized by broadening of the R_g distribution for Q15 vis-à-vis Q5 (Fig. 4). This increase in conformational heterogeneity implies an ensemble characterized by large fluctuations — a feature that has direct bearing on the increase in likelihood of nucleating β -sheets with increasing chain lengths.

In the EV limit, the scaling of R_g with chain length can be written as $R_g = R_0 N^{0.59}$.^{86,88,95} Unlike denatured proteins which obey the scaling laws for chains in the EV limit,⁹⁴ the ensemble for disordered polyglutamine in water is, on average, much more compact [Figs. 3(b,d) and 4]. To compute the requisite scaling exponent and average packing density we will need to carry out simulations for several chain lengths including very long chains. This analysis is part of ongoing work. A discussion of two possibilities for monomeric polyglutamine follows.

In accordance with the behavior of folded, globular proteins, which are akin to chains in a poor solvent, the radius of gyration for monomeric polyglutamine could scale as, $R_g = R_0 N^{0.34}$.⁹⁵ If this scaling applies, then polyglutamine prefers to be collapsed or crumpled⁹⁶ without showing a discernible preference for a specific backbone conformation. If so, the mechanism of β -sheet nucleation involves a conformational transition on the manifold of compact states.⁹⁵ It is also possible that the disordered ensemble is such that chain-chain repulsions exactly counterbalance chain-chain attractions. For this case $R_g = R_0 N^{0.5}$ and polyglutamine would behave like a flexible, unperturbed chain in a so-called theta state.⁸⁸ However, the ensemble average value of δ is 0.29 for Q15, which is consistent with a spheroid rather than an ellipsoid or a rod.⁸⁴ The Q15 peptide is a likely indicator of the average shape for longer peptides. Hence, the current data would appear to exclude the theta state as a possibility because $\delta > 0.6$ for a chain in the theta state.⁸⁶ Therefore, it appears that polyglutamine in water is a statistical coil

in a poor solvent in that it is compact with access to a heterogeneous distribution of backbone conformations.

Regular Local Conformations

We analyzed the ensembles of Q5 and Q15 in water to assess quantitative preferences for canonical local secondary structures such as α -helices, β -strands, and polyproline II (P_{II}) helices. These structures come about when consecutive stretches of backbone (ϕ, ψ)-angles adopt similar values. To assay for regular local structures we use the PROSS algorithm.⁹⁷ This is a method for secondary structure assignment based solely on backbone (ϕ, ψ)-angles. The results are tabulated in Table II. For a given peptide, the numbers shown in Table II quantify the probability of finding a conformation with at least three consecutive residues adopting (ϕ, ψ)-angles compatible with either regular α -helices, regular β -strands, or regular P_{II} -helices. It is clear that these probabilities vary with chain length. However, for a chain of a given length, the probabilities for accessing short stretches of different canonical regular conformations are similar to each other. The conclusion is that by this low-resolution assay for structure, no single regular conformation dominates. In the parlance of energy landscape theory,⁸³ we propose that the landscape is like an egg-carton showing signatures of maximal frustration.⁹⁸

Conformational Propensities

In Figure 5(a,b) we compare the conformational propensities of individual residues extracted from the Q5 and Q15 peptides, which are shown as Ramachandran (contour) maps.⁹⁹ For a given residue in Q5 or Q15, contour maps are constructed by picking conformations from an ad hoc cluster [Fig. 3(a,b)] and tabulating the residue-specific probabilities for accessing distinct regions within (ϕ, ψ)-space.

Results for Q5

Figure 5(a) shows (ϕ, ψ)-maps for all residues of the Q5 peptide using conformations drawn from all four ad hoc regions of (δ, R_g)-space. For conformations drawn from box 1 there is a clear preference for α -helical (ϕ, ψ)-angles. This implies a preference for either a single turn of α -helix or for Type I helical turns. Conversely, for conformations drawn from box 4 there is a marked preference for P_{II} -like

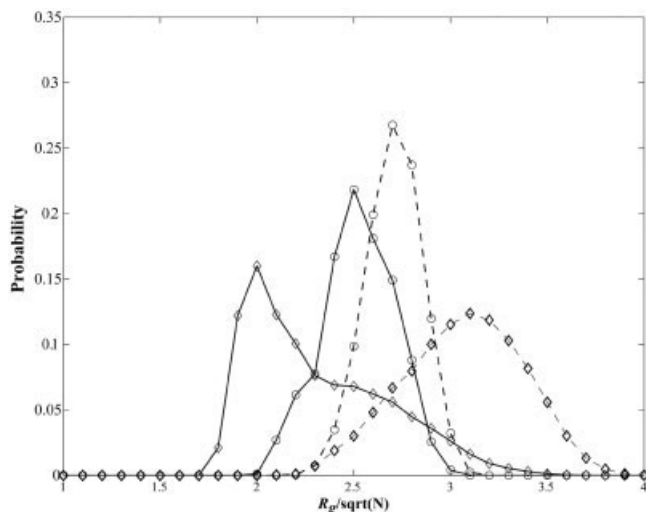


Fig. 4. Comparison of probability distributions of radii of gyration. Here N denotes chain length. Four curves are shown. These include Q5 in water (\circ), Q15 in water (\diamond), Q5 in the EV limit (\circ), and Q15 in the EV limit (\diamond).

TABLE II. Probability (%) of Finding a Conformation with Regular Local Structure*

| | α -Helix | β -Strand | P_{II} -Helix |
|--------------|------------------|------------------|------------------|
| Q5 in water | 4.24 ± 0.45 | 4.19 ± 0.20 | 6.32 ± 0.36 |
| Q15 in water | 13.49 ± 1.44 | 12.13 ± 0.87 | 16.71 ± 0.88 |

*Regular structures are assayed using PROSS algorithm.⁹⁷ All errors are standard errors estimated from the bootstrap analysis.

(ϕ, ψ) -angles. Although the intrinsic propensity of glutamine for P_{II} and α -helical (ϕ, ψ) -angles is high and consistent with experimental data¹⁰⁰ this does not result in an ensemble that is a simple combination of regular P_{II} and α -helices. Instead, irregular conformations that are realized by combinations of the two types of (ϕ, ψ) -angles are the norm. This is quantified in terms of the populations associated with boxes 2 and 3 for Q5 [Fig. 3(a)] — the two regions that account for approximately 70% of the Q5 conformational ensemble (Table I). From analysis of the Q5 dihedral angle distributions we conclude that helical turns and bends derived by irregular combinations of α -helical and P_{II} (ϕ, ψ) -angles dominate the ensemble for the Q5 peptide.

Results for Q15

As a point of comparison, we show in Figure 5(b) (ϕ, ψ) -maps for the five central amino acids of the Q15 peptide. Data in Table I indicate that for Q15 there is a greater preference for conformations that are compact and globular versus those that are extended. There is an approximately 70% chance of finding the peptide in the regions 1 and 2 shown in Figure 3(b). Conformations drawn from these regions are compact and loosely packed globules and there is an increased propensity for forming Type II turns. The latter is evidenced by the increased accessibility for positive ϕ -angles, especially left-handed

α -helix (ϕ, ψ) -angles, which in combination with the intrinsic propensity for the P_{II} region leads to the formation of β -turns [Fig. 5(b)].

β -Sheet Formation in Q15

Although the probability of forming β -turns is finite and quantifiable, the overall likelihood of sampling regular β -sheet geometries remains small. This is because the tendency toward disorder, driven by the intrinsic propensity for different regions of (ϕ, ψ) -space, promotes the sampling of diverse backbone conformations. In other words, there exists an entropic bottleneck to accessing β -sheet geometries. This bottleneck can be overcome and statistical fluctuations do lead to a small but real probability that the Q15 peptide accesses antiparallel β -sheets. We estimate this probability to be between 0.1 and 2%. In Figure 6 we show representative structures drawn from each ad hoc region of the two-dimensional order parameter space identified in Figure 3(b). It is clear that when the chain is compact there is a finite probability of adopting antiparallel β -sheet geometries. Not surprisingly, it is nearly impossible to nucleate any kind of β -sheet structure for the Q5 peptide. Even for Q15, the small likelihoods associated with β -sheet structures implies that interactions which promote conformational heterogeneity compete with β -sheet formation. We now proceed to identify the interactions that promote conformational heterogeneity and hence a disordered ensemble.

Why are the Ensembles for Q5 and Q15 Disordered?

The Q5 ensemble is disordered because the peptide is too short to realize cooperative transitions into ordered, regular secondary structures. We focus our analysis on the Q15 ensemble and quantify the average number of hydrogen bonds (backbone–backbone, backbone–sidechain, and sidechain–sidechain) found in different conformations accessible in the disordered ensemble.

In general, a Q15 conformation drawn from any of the four conformational regions, shown in Figure 3(b), will have more sidechain–backbone hydrogen bonds than either of the other two types. This is shown in Figure 7, which plots the average number of hydrogen bonds per conformation realized in each region identified in Figure 3(b).

Sidechain–backbone hydrogen bonds are realizable in a wide variety of backbone geometries, including compact globules and extended geometries. Additionally, these hydrogen bonds can be both local and nonlocal. This is illustrated in Figure 8, where we show four dissimilar backbone conformations, all of which have four sidechain–backbone hydrogen bonds. The backbone peptide units are

Fig. 5. Ramachandran plots shown as contour maps in (ϕ, ψ) -space. (a): Contour maps are shown for each of the five residues of the Q5 peptide. Each row corresponds to conformations extracted from an ad hoc cluster identified in Figure 3. (b): Ramachandran maps for the five central residues of the Q15 peptide. Each row corresponds to conformations extracted from an ad hoc cluster identified in Figure 3. In both sets of plots the color bar for each row is situated at the end of the row.

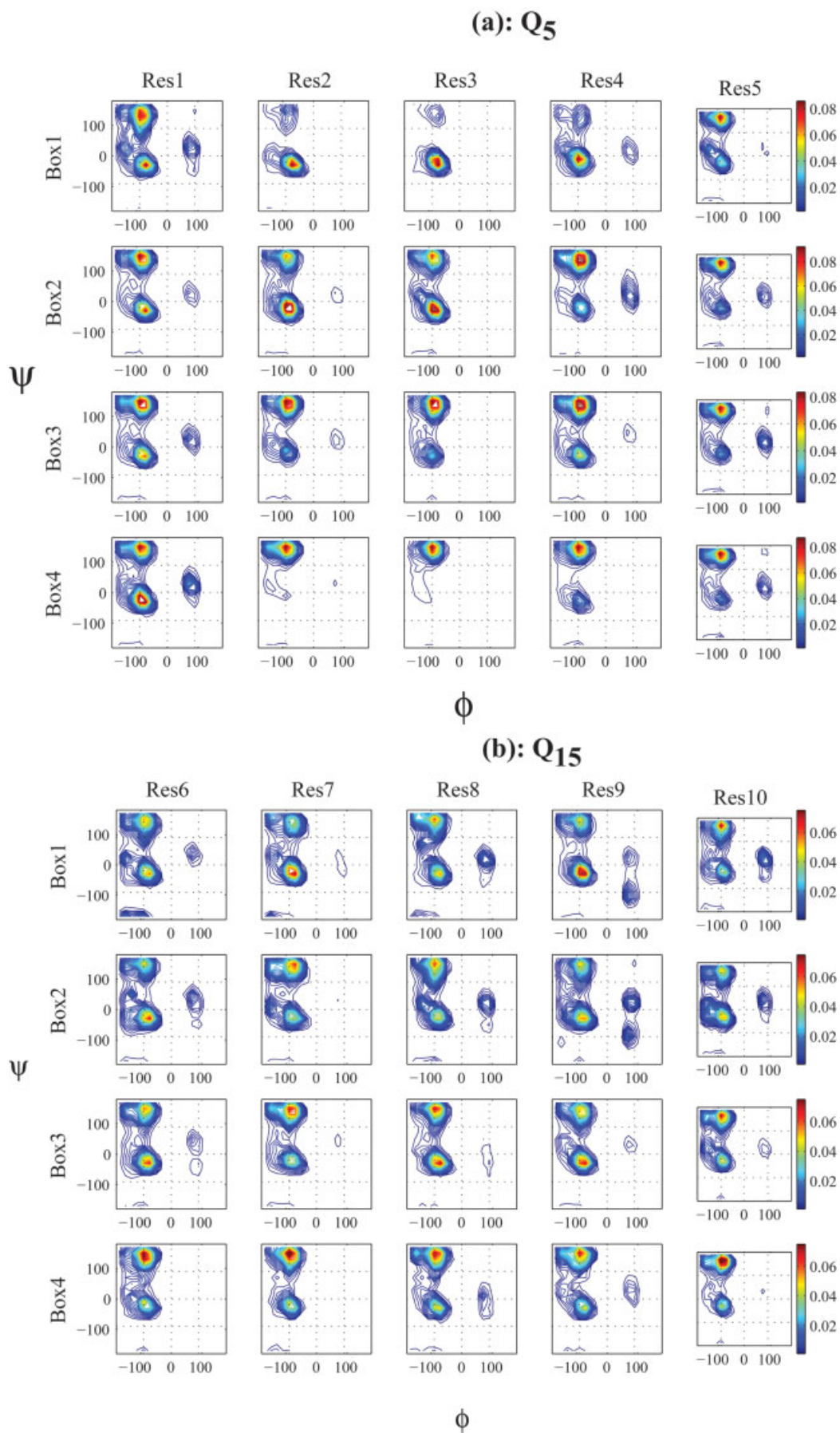


Figure 5.

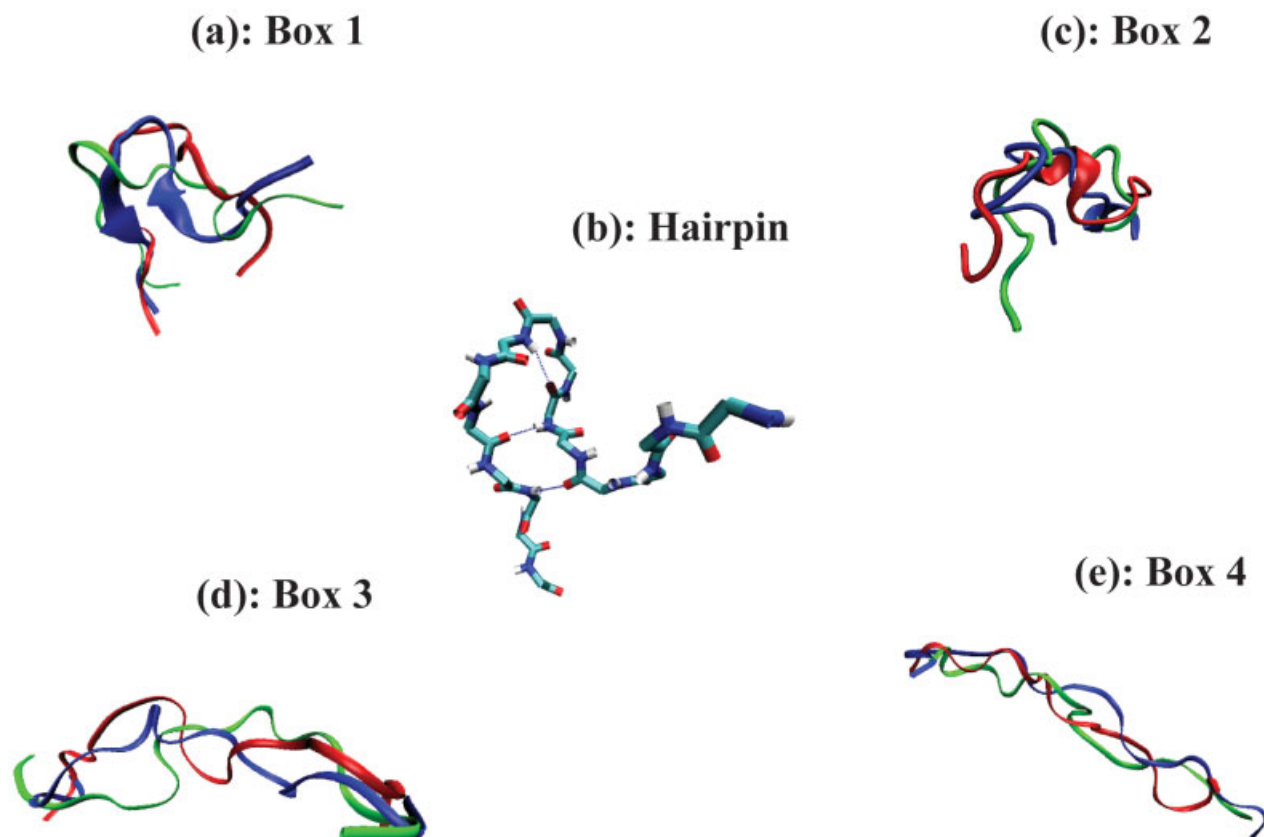


Fig. 6. Representative conformations drawn from the different regions (boxes 1–4) of the order parameter space identified in Figure 3(b). The pictures are meant purely for illustration only. No quantitative statistics are to be ascribed to these snapshots. Figure 6(b) illustrates the fact that statistical fluctuations can lead to a sampling of β -sheet geometries that are akin to a β -hairpin with antiparallel strands.

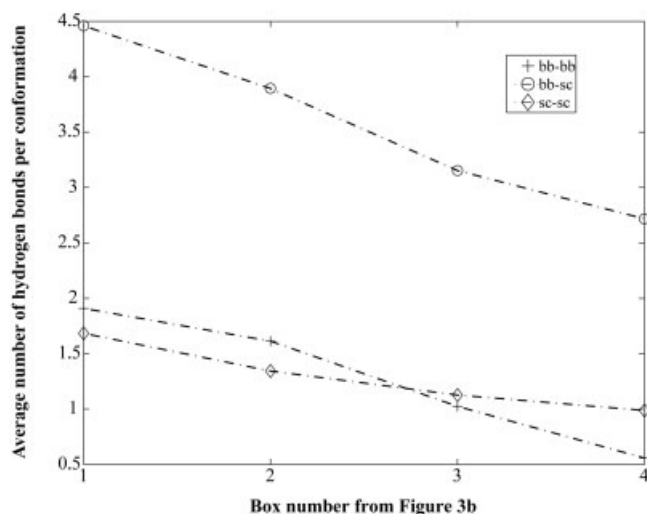


Fig. 7. Average number of hydrogen bonds per conformation extracted from the four ad hoc clusters identified for Q15. Data shown are for backbone–backbone (+), sidechain–backbone (o), and sidechain–sidechain (\diamond) hydrogen bonds. The dashed-dotted lines (–) serve as visual aids.

predominantly solvated by way of hydrogen bonds to the polar sidechain or through surrounding water molecules and these modes of backbone solvation are not restricted to

a specific backbone conformation. The conclusion is that Q15 is disordered because sidechain–backbone hydrogen bonds can form almost anywhere along the chain and in any of the conformations accessible to Q15.

Eberhardt and Raines¹⁰¹ showed that 25.2*M*-formamide is almost as good as 55.5*M*-water in terms of its ability to form hydrogen bonds with backbone peptide units. Formamide, which is a primary amide, mimics polar moieties in the sidechains of glutamine and asparagine. In polyglutamine the effective concentration of the sidechain primary amide around the backbone peptide unit is always high because the polar moiety is covalently attached to the backbone. Hence, the glutamine sidechain can compete with water as an alternative solvent and form hydrogen bonds to the backbone. This increases the number of different modes for solvating the backbone. Consequently, the probability associated with any specific backbone conformation decreases and this in turn promotes backbone disorder.

What are the Implications for β -sheet Nucleation?

In addition to providing an explanation for the observed disorder, the conformation-independent probability of realizing multiple sidechain–backbone hydrogen bonds also leads to a hypothesis for why β -sheet formation is postulated to be a highly unfavorable thermodynamic reaction.¹

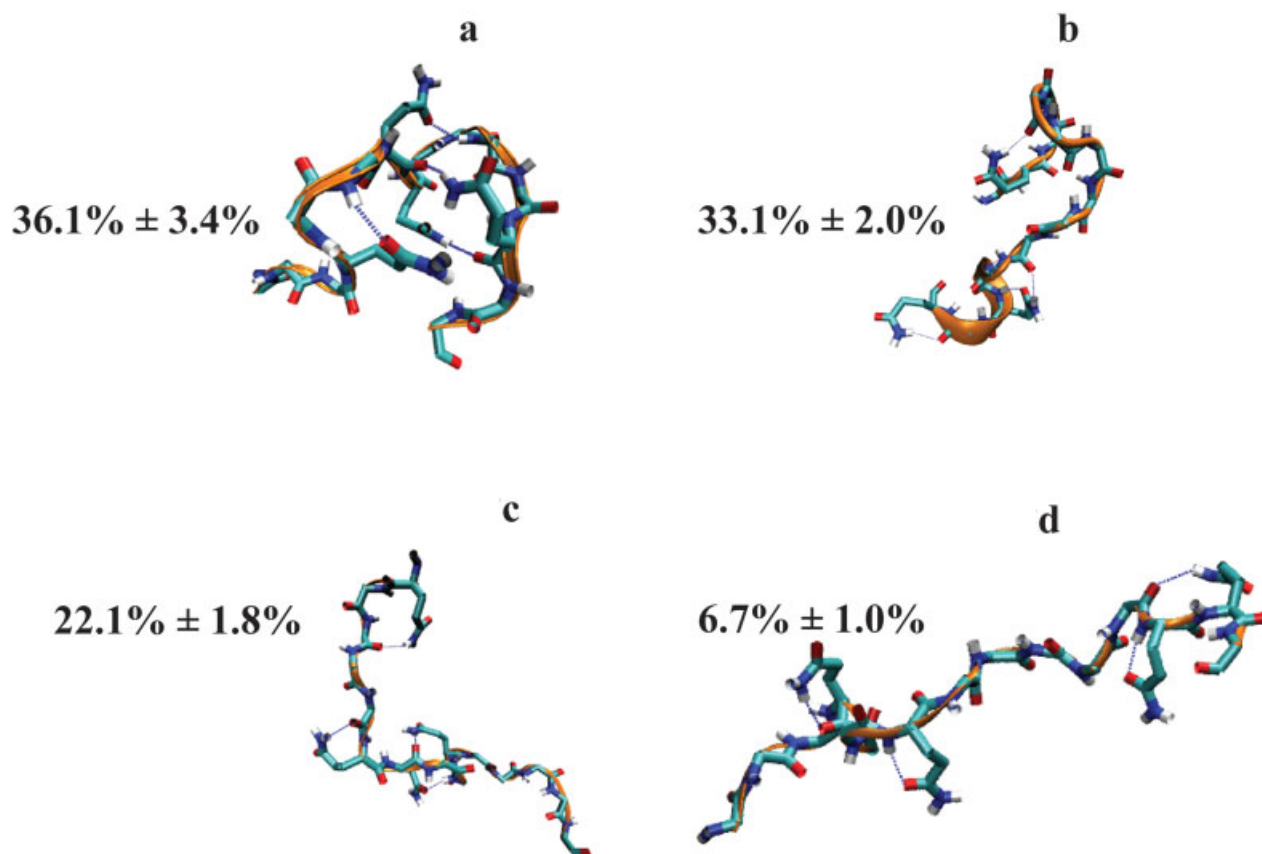


Fig. 8. Four disparate conformations each with four sidechain–backbone hydrogen bonds. Sidechain atoms are depicted only for those residues that participate in sidechain–backbone hydrogen bonds. Blue dotted lines indicate sidechain–backbone hydrogen bonds. In all pictures the gold colored ribbon identifies the backbone. Numbers (%) shown next to each conformation refer to the percentage probabilities associated with the ad hoc cluster from which the conformation is drawn.

Classic secondary structures are characterized by backbone–backbone hydrogen bonds that require a regular repeat of (ϕ, ψ) -angles.¹⁰² In the case of β -sheets there is an additional need for the appropriate registry of β -strands. The possibility of realizing sidechain–backbone hydrogen bonds almost anywhere along the homopolymeric chain interferes with the cooperativity of interactions required for transitioning into regular secondary structures,¹⁰³ since a large fraction of peptide units become unavailable for cooperative backbone–backbone interactions. Consequently, the probability of adopting conformations in which the backbone solvates itself via backbone–backbone hydrogen bonds is very small. For example, the probability of finding an individual glutamine in α -helical or P_{II} -like (ϕ, ψ) value is high (Fig. 5). Sidechain–backbone hydrogen bonds contribute to these high intrinsic propensities (data not shown). Intrinsic propensities facilitate the formation of bends and turns. However, it is not easy to localize these bends and turns to a specific part of the homopolymeric polyglutamine sequence. Additionally, the high intrinsic propensity for P_{II} - and α -helical (ϕ, ψ) values interferes with strand propagation. This in turn makes it difficult to realize the correct registry of strands required for backbone–backbone hydrogen bonding. Our model provides a

plausible explanation for the strong chain length dependent aggregation of polyglutamine peptides.

Support for these observations comes from the mutational analysis of Thakur and Wetzel⁴⁴ who showed that sequences of the form (Q9PG)₄ and (Q10PG)₄ undergo spontaneous aggregation, whereas sequences of the form (Q7PG)₄ and (Q8PG)₄ do not aggregate as readily. Furthermore, the sequence (P_DGQ9), where P_D is D-proline enhances the aggregation rate vis-a-vis the sequences with L-proline. Ross and coworkers have arrived at similar conclusions using mutational analysis of the exon 1 fragment of huntingtin.¹⁰⁴ These data are suggestive of a minimum length requirement for extended β -strands. Insertion of turn forming amino acids in locations that interrupt the disordering tendencies of polyglutamine appear to pre-pay some of the entropic penalty that opposes β -sheet nucleation.

DISCUSSION

Summary

We have used multiple molecular dynamics simulations to characterize the conformational ensemble of monomeric polyglutamine for two peptides, Q5 and Q15. Consistent with expectations from CD data, we have shown that the

ensembles for both peptides are disordered. However, there are quantifiable differences between the two ensembles and in particular as chain length increases there is an increased probability of sampling more compact geometries. Furthermore, fluctuations for Q15 are greater than for Q5 as evidenced by the broadening of the distribution shown in Figure 4.

We showed that a typical Q15 conformation has on average four to five sidechain–backbone hydrogen bonds (Fig. 7). This is true irrespective of whether the conformations are compact, semi-compact, or extended (Fig. 8). Sidechain–backbone hydrogen bonds can furthermore be local or non-local. Conformations in the disordered ensemble are solvated by hydrogen bonds to sidechain polar groups or surrounding water molecules. The multiplicity of alternative (non backbone–backbone) hydrogen bonding possibilities provides an insight into why β -sheet formation is thermodynamically unfavorable.

Nucleation of β -sheet, a process which requires a change in solvation state whereby the backbone solvates itself, requires that a conformational entropy bottleneck be overcome. This bottleneck is based on the nearly conformation-independent probability of realizing sidechain–backbone hydrogen bonds in polyglutamine tracts. In short, we propose that swapping so many sidechain–backbone or water–backbone hydrogen bonds for backbone–backbone hydrogen bonds is opposed by conformational entropy.

It should be noted that it is more than likely that our observations will vary if we were to use a different force field.¹⁰⁵ Hence, the robustness of our conclusions can only be assayed by carrying out similar simulations using a cross-section of force fields and water models — an expensive, yet important proposition.

It is imperative to remind the reader that at the requisite concentrations (ca. $10\mu M$) long polyglutamine peptides aggregate to form β -sheet rich aggregates. β -sheet aggregates are expected to be thermodynamically preferred states at high concentrations. The fact that monomeric polyglutamine is predominantly unfolded in solution leaves it susceptible to folding via aggregation. The question of interest is why is folding or β -sheet formation thermodynamically unfavorable for monomeric polyglutamine? The foregoing analysis provides a plausible explanation for why monomeric polyglutamine prefers to be disordered in solution.

β -helices versus antiparallel β -sheets? We find that statistical fluctuations can lead to a sampling of β -sheet geometries for Q15 (Fig. 6). Because it is relatively easy to sample bends and turns, there is a small but finite probability of accessing antiparallel β -sheets. This is important in light of two different interpretations of fiber diffraction data for a D2Q15K2 peptide. Perutz and coworkers¹¹ proposed that the data were consistent with the peptide adopting a β -helical structure that gives rise to a water-filled nanotube for the amyloid fiber. Recently Sikorski and Atkins¹⁰⁶ reinterpreted these data and concluded that the data appear to be consistent with a once folded hairpin conformation. The trends seen in our simulations [Fig. 6(b)], provide tentative and independent support for

the model of Sikorski and Atkins.¹⁰⁶ However, results from coarse-grain simulations¹⁰⁷ and shorter molecular dynamics simulations¹⁰⁸ appear to lend support for the parallel β -helix model while data for aggregation kinetics are consistent with both structural models.²⁶

Pending the availability of data of the kind shown in this work for longer polyglutamine peptides, we are forced to remain agnostic about the types of β -sheet structures accessible to polyglutamine peptides. This is an important issue to resolve because it is reasonable to assume that β -sheet structures sampled by the monomer²⁶ — the nucleus for aggregation — are related to the structure of the monomer in the context of the aggregate. Alternatively, it is also conceivable that heterogeneity in monomeric β -sheet structures could explain the diversity of oligomeric structures observed by Muchowski and coworkers⁴⁰ for aggregates of polyglutamine expansions.

Connection to Theories and Ongoing Work

The finding of Wetzel and coworkers that the monomer acts as the nucleus¹ for aggregation is significant because there are theories for β -sheet nucleation that allow one to calculate the free energy for β -sheet formation as a function of chain length.¹⁰⁹

Finkelstein¹⁰⁹ has estimated the minimal length N^* of an unstable intermediate to be $N^* \approx \frac{F_t}{(-\Delta F_\beta)}$. Here F_t is the free energy of a turn/bend/loop that connects adjacent strands of a sheet and $\Delta F_\beta = F_\beta - F_c$ is the free energy change for a transition from coil to β -sheet. The length N^* is estimated by stipulating that for $N = N^*$ the free energy gain from addition of a strand compensates the free energy lost for nucleating a turn. Interestingly, in this theory there is a chain length past which the β -sheet is the stable entity — a situation that does not appear to hold for monomeric polyglutamine. Finkelstein¹⁰⁹ notes that conformational heterogeneity in the coil state will profoundly influence both the sign and magnitude of ΔF_β .

We propose that sidechain–backbone hydrogen bonds leads to frustration⁸³ in that ΔF_β can never be less than zero for monomeric polyglutamine irrespective of chain length although the relative values of ΔF_β decrease with increasing chain length. To test this hypothesis we need robust estimates of $\Delta R; F_\beta$ for polyglutamine as a function of chain length. This will require quantitative knowledge of length-dependent changes in PDFs for longer polyglutamine chains and significant enhancement in sampling including the use of replica exchange^{49,52,59} and other multiplexing¹¹⁰ strategies. This work is ongoing.

ACKNOWLEDGMENTS

We thank Ronald Wetzel and Nathan Baker for stimulating discussions and James Bann for drawing our attention to data in reference 101. We dedicate this paper to George Rose on the occasion of his 65th birthday.

REFERENCES

1. Chen S, Ferrone FA, Wetzel R. Huntington's disease age-of-onset linked to polyglutamine aggregation nucleation. *Proc Natl Acad Sci U S A* 2002;99:11884–11889.

2. Harper PS. Huntington's disease: a clinical, genetic, and molecular model for polyglutamine repeat disorders. In: Harper PS, Perutz M. editors. *Glutamine repeats and neurodegenerative diseases: molecular aspects*. Oxford: Oxford University Press; 2001. p 1–9.
3. Wilmot GR, Warren ST. A new mutational basis for disease. In: Wells RD, Warren ST, editors. *Genetic instabilities and hereditary neurological diseases*. San Diego: Academic Press; 1998. p 3–12.
4. Gusella JF, McDonald ME. Huntingtin: a single bait hooks many species. *Curr Opin Neurobiol* 1998;8:425–430.
5. Cummings CJ, Zoghbi HY. Fourteen and counting: unraveling trinucleotide repeat diseases. *Hum Mol Genet* 2000;9:909–916.
6. Bates GP, Bann C. The polyglutamine diseases. In: Bates GP, Harper PS, Jones L, editors. *Huntington's disease*. Oxford: Oxford University Press; 2002. p 429–472.
7. Scherzinger E, Wanker EE, Mangiarini L, Bates GP. Formation of neuronal intranuclear inclusions (NII) underlies the neurological dysfunction in mice transgenic for the HD mutation. *Cell* 1997;90:537–548.
8. Becher MW, Kotzok JA, Sharp AH, Davies SW, Bates GP, Price DL, Ross CA. Intranuclear neuronal inclusions in Huntington's disease and dentatorubral pallidolysian atrophy: correlation between density of inclusions and IT15 CAG repeat length. *Neurobiol Dis* 1998;4:387–395.
9. Davies SW, Turmaine M, Cozens BA, Raza AS, Mahal A, Mangiarini L, Bates GP. From neuronal inclusions to neurodegeneration: neuropathological investigation of a transgenic mouse model of Huntington's disease. *Philos Trans R Soc London B* 1999;354:971–979.
10. Perutz MF, Finch JT, Berriman J, Lesk A. Amyloid fibers are water-filled nanotubes. *Proc Natl Acad Sci U S A* 2002;99:5591–5595.
11. Ross CA, Poirier MA, Wanker EE, Amzel M. Polyglutamine fibrillogenesis: the pathway unfolds. *Proc Natl Acad Sci U S A* 2003;100:1–3.
12. Chen S, Berthelie V, Hamilton JB, O'Neill B, Wetzel R. Amyloid-like features of polyglutamine aggregates and their assembly kinetics. *Biochemistry* 2002;41:7391–7399.
13. Yang W, Dunlap JR, Andrews RB, Wetzel R. Aggregated polyglutamine peptides delivered to nuclei are toxic to mammalian cells. *Hum Mol Genet* 2002;11:2905–2917.
14. Rochet JC, Lansbury PT. Amyloid fibrillogenesis: themes and variations. *Curr Opin Struct Biol* 2000;10:60–68.
15. Wanker EE. Protein aggregation and pathogenesis of Huntington's disease: mechanisms and correlations. *Biol Chem* 2000;381:937–942.
16. Ross CA. Polyglutamine pathogenesis: emergence of unifying mechanisms for Huntington's disease and related disorders. *Neuron* 2002;35:819–822.
17. Sacchettini JC, Kelly JW. Therapeutic strategies for human amyloid diseases. *Nature Rev Drug Discovery* 2002;1:267–275.
18. Serio TR, Lindquist SL. The yeast prion [PSI⁺]: molecular insights and functional consequences. *Adv Protein Chem* 2002;59:391–412.
19. Caughey B, Lansbury PT. Protofibrils, pores, fibrils, and neurodegeneration: separating the responsible protein aggregates from the innocent bystanders. *Annu Rev Neurosci* 2003;26:267–298.
20. Huff ME, Balch WE, Kelly JW. Pathological and functional amyloid formation orchestrated by the secretory pathway. *Curr Opin Struct Biol* 2003;13:674–682.
21. Vendruscolo M, Zurdo J, MacPhee CE, Dobson CM. Protein folding and misfolding: a paradigm of self-assembly and regulation in complex biological systems. *Phil Trans Royal Soc A* 2003;361:1205–1222.
22. Dobson CM. Protein folding and misfolding. *Nature* 2003;426:884–890.
23. Dobson CM. Principles of protein folding, misfolding and aggregation. *Semin Cell Dev Biol* 2004;15:3–16.
24. Ohnishi S, Takano K. Amyloid fibrils from the viewpoint of protein folding. *Cell Mol Life Sci* 2004;61:511–524.
25. Uversky VN, Fink AL. Conformational constraints for amyloid fibrillation: the importance of being unfolded. *Biochim Biophys Acta Proteins Proteomics* 2004;1698:131–153.
26. Wetzel R. Protein folding and aggregation in the expanded polyglutamine repeat diseases. In: Buchner J, Kiefhaber T, editors. *Protein folding handbook*. Weinheim, Germany: Wiley-VCH; 2005. p 1200–1244.
27. Chiti F, Stefani M, Taddei N, Ramponi G, Dobson CM. Rationalization of the effects of mutations on peptide and protein aggregation rates. *Nature* 2003;424:805–808.
28. Dubay KF, Pawar AP, Chiti F, Dobson CM, Vendruscolo M. Prediction of the absolute aggregation rates of amyloidogenic polypeptide chains. *J Mol Biol* 2004;341:1317–1326.
29. Marchesi VT. An alternative interpretation of the amyloid A beta hypothesis with regard to the pathogenesis of Alzheimer's disease. *Proc Natl Acad Sci U S A* 2005;102:9093–9098.
30. Reixach N, Deechongkit S, Jiang X, Kelly JW, Buxbaum JN. Tissue damage in the amyloidoses: transthyretin monomers and nonnative oligomers are the major cytotoxic species in tissue culture. *Proc Natl Acad Sci U S A* 2004;101:2817–2822.
31. Kaye R, Head E, Thompson JL, McIntire TM, Milton SC, Cotman CW, Glabe CG. Common structure of soluble amyloid oligomers implies common mechanism of pathogenesis. *Science* 2003;300:486–489.
32. Sanchez I, Mählke C, Yuan JY. Pivotal role of oligomerization in expanded polyglutamine neurodegenerative disorders. *Nature* 2003;421:373–379.
33. Poirier MA, Li H, Macosko J, Cai S, Amzel M, Ross CA. Huntingtin spheroids and protofibrils as precursors in polyglutamine fibrillogenesis. *J Biol Chem* 2002;277:41032–41037.
34. El-Agnaf OMA, Mahil DS, Patel BP, Austen BM. Oligomerization and toxicity of beta-amyloid-42 implicated in Alzheimer's disease. *Biochem Biophys Res Commun* 2000;273:1003–1007.
35. Pillai VNR, Mutter M. Conformational studies of poly(oxyethylene)-bound peptides and protein sequences. *Acc Chem Res* 1981;14:122–130.
36. Tuchscherer G, Mutter M. Under the influence of Phi and Psi. *J Pept Sci* 2005;11:278–282.
37. Scherzinger E, Sittler A, Schweiger K, Heiser V, Lurz R, Hasenbank R, Bates GP, Lehrach H, Wanker EE. Self-assembly of polyglutamine-containing huntingtin fragments into amyloid-like fibrils: implications for Huntington's disease pathology. *Proc Natl Acad Sci U S A* 1999;96:4604–4609.
38. Bennett MJ, Huey-Tubman KE, Herr AB, West AP, Ross SA, Bjorkman PJ. A linear lattice model for polyglutamine in CAG-expansion diseases. *Proc Natl Acad Sci U S A* 2002;99:11634–11639.
39. Masino L, Kelly G, Leonard K, Trottier Y, Pastore A. Solution structure of polyglutamine tracts in GST-polyglutamine fusion proteins. *FEBS Lett* 2002;513:267–272.
40. Wacker JL, Zareie MH, Fong H, Sarikaya M, Muchowski PJ. Hsp70 and Hsp40 attenuate formation of spherical and annular polyglutamine oligomers by partitioning monomer. *Nature Struct Molec Biol* 2004;11:1215–1222.
41. Perutz MF, Johnson T, Suzuki M, Finch JT. Glutamine repeats as polar zippers: their possible role in inherited neurodegenerative diseases. *Proc Natl Acad Sci U S A* 1994;91:5355–5358.
42. Altschuler EL, Hud NV, Mazrimas JA, Rupp B. Random coil conformation for extended polyglutamine stretches in aqueous soluble monomeric peptides. *J Pept Res* 1997;50:73–75.
43. Chen S, Berthelie V, Yang W, Wetzel R. Polyglutamine aggregation behavior in vitro supports a recruitment mechanism of cytotoxicity. *J Mol Biol* 2001;311:173–182.
44. Thakur AK, Wetzel R. Mutational analysis of the structural organization of polyglutamine aggregates. *Proc Natl Acad Sci U S A* 2002;99:17014–17019.
45. Greenfield N, Fasman GD. Computed circular dichroism spectra for the evaluation of protein conformation. *Biochemistry* 1969;8:4108–4116.
46. Chen YW. Local protein unfolding and pathogenesis of polyglutamine-expansion diseases. *Proteins* 2003;51:68–73.
47. Kashchiev, D. *Nucleation*. Oxford, UK: Butterworth; 2000. Chap 2–5.
48. Guo Z, Brooks III CL, Boczek EM. Exploring the folding free energy surface of a three-helix bundle. *Proc Natl Acad Sci U S A* 1997;94:10161–10166.
49. Mitsutake A, Okamoto Y. Replica-exchange simulated tempering method for simulations of frustrated systems. *Chem Phys Lett* 2000;332:131–138.
50. Shirts MR, Pande VS. Mathematical analysis of coupled parallel simulations. *Phys Rev Lett* 2001;86:4983–4987.
51. Shea JE, Brooks III CL. From folding theories to folding proteins: a review and assessment of simulation studies of protein folding and unfolding. *Annu Rev Phys Chem* 2001;52:499–535.

52. Nymeyer H, Gnanakaran S, García AE. Atomic simulations of protein folding using the replica exchange algorithm. *Methods Enzymol* 2004;383:119–149.
53. Sheinerman FB, Brooks III CL. Calculations on folding of segment B1 of streptococcal protein G. *J Mol Biol* 1998;278:439–456.
54. Ferrara P, Apostolakis J, Caffisch A. Thermodynamics and kinetics of folding of two model peptides investigated by molecular dynamics simulations. *J Phys Chem B* 2000;104:5000–5010.
55. Hiltpol A, Ferrara P, Gsponer J, Caffisch A. Free energy surface of the helical peptide Y(MEARA)6. *J Phys Chem B* 2000;104:10080–10086.
56. Pande VS, Baker I, Chapman J, Elmer SP, Khaliq S, Larson SM, Rhee YM, Shirts MR, Snow CD, Sorin EJ, Zagrovic B. Atomistic protein folding simulations on the submillisecond time scale using worldwide distributed computing. *Biopolymers* 2003;68:91–109.
57. Klimov DK, Thirumalai D. Dissecting the assembly of A beta(16–22) amyloid peptides into antiparallel beta sheets. *Structure* 2003;11:295–307.
58. Paci E, Gsponer J, Salvatella X, Vendruscolo M. Molecular dynamics studies of the process of amyloid aggregation of peptide fragments of transthyretin. *J Mol Biol* 2004;340:555–569.
59. Wei GH, Mousseau N, Derreumaux P. Sampling the self-assembly pathways of KFFE hexamers. *Biophys J* 2004;87:3648–3656.
60. Melquiond A, Boucher G, Mousseau N, Derreumaux P. Following the aggregation of amyloid-forming peptides by computer simulations. *J Chem Phys* 2005;122:174904.
61. Tsai H-H, Rechtes M, Tsai C-J, Gunasekaran K, Gazit E, Nussinov R. Energy landscape of amyloidogenic peptide oligomerization by parallel-tempering molecular dynamics simulation: significant role of Asn ladder. *Proc Natl Acad Sci U S A* 2005;102:8174–8179.
62. Pappu RV, Srinivasan R, Rose GD. The Flory isolated pair hypothesis is not valid for polypeptide chains: implications for protein folding. *Proc Natl Acad Sci U S A* 2000;97:12565–12570.
63. Zagrovic B, Pande VS. Structural correspondence between the alpha-helix and the random-flight chain resolves how unfolded proteins can have native-like properties. *Nat Struct Biol* 2003;10:955–961.
64. Finke JM, Cheung MS, Onuchic JN. A structural model of polyglutamine determined from a host-guest method combining experiments and landscape theory. *Biophys J* 2004;87:1900–1918.
65. Garcia AE. Characterization of non-alpha helical conformations in Ala peptides. *Polymer* 2004;45:669–676.
66. Day R, Daggett V. All-atom simulations of protein folding and unfolding. *Adv Protein Chem* 2003;66:373–403.
67. Zaman MH, Shen M-Y, Berry RS, Freed KF, Sosnick TR. Investigations into sequence and conformational dependence of backbone entropy, inter-basin dynamics and the Flory isolated-pair hypothesis for peptides. *J Mol Biol* 2003;331:693–711.
68. Tran HT, Wang X, Pappu RV. Reconciling observations of sequence specific conformational propensities with the generic polymeric behavior of denatured proteins. *Biochemistry* 2005;44:11369–11380.
69. Jorgensen WL, Maxwell DS, Tirado-Rives J. Development and testing of the OPLS all-atom force field on conformational energetics and properties of organic liquids. *J Am Chem Soc* 1996;117:11225–11236.
70. Jorgensen WL, Tirado-Rives J. Potential energy functions for atomic-level simulations of water and organic and biomolecular systems. *Proc Natl Acad Sci U S A* 2005;102:6665–6670.
71. Jorgensen WL, Jenson C. Temperature dependence of TIP3P, SPC, and TIP4P water from NPT Monte Carlo simulations: seeking temperatures of maximum density. *J Comput Chem* 1998;19:1179–1186.
72. Berendsen HJC, van der Spoel D, van Drunen R. GROMACS: a message-passing parallel molecular dynamics implementation. *Comp Phys Commun* 1995;91:43–56.
73. Lindahl E, Hess B, van der Spoel D. GROMACS 3.0: a package for molecular simulation and trajectory analysis *J Mol Model* 2001;7:306–317.
74. Berendsen HJC, Postma JPM, van Gunsteren WF, DiNola A, Haak JR. Molecular dynamics with coupling to an external bath. *J Chem Phys* 1984;81:3684–3690.
75. Hess B, Bekker H, Berendsen HJC, Fraaije JGEM. LINCS: a linear constraint solver for molecular simulations. *J Comput Chem* 1997;18:1463–1472.
76. York DM, Wlodawer A, Pedersen LG, Darden TA. Atomic-level accuracy in simulations of large protein crystals. *Proc Natl Acad Sci U S A* 1994;91:8715–8718.
77. Weber W, Hunenberger PH, McCammon JA. Molecular dynamics simulations of a polyalanine octapeptide under Ewald boundary conditions: influence of artificial periodicity on peptide conformation. *J Phys Chem B* 2000;104:3668–3675.
78. Drozdov AN, Grossfield A, Pappu RV. The role of solvent in determining conformational preferences of alanine dipeptide in water. *J Am Chem Soc* 2004;126:2574–2581.
79. Mountain RD, Thirumalai D. Molecular dynamics simulations of end-to-end contact formation in hydrocarbon chains in water and aqueous urea solution. *J Am Chem Soc* 2003;125:1950–1957.
80. Swope WC, Pitera JW, Suits F. Describing protein folding kinetics by molecular dynamics simulations. 1. Theory. *J Phys Chem B* 2004;108:6571–6581.
81. Swope WC, Pitera JW, Suits F, Pitman M, Eleftheriou M, Fitch BG, Germain RS, Rayshubski A, Ward TJC, Zhestkov Y, Zhou R. Describing protein folding kinetics by molecular dynamics simulations. 2. Example applications to alanine dipeptide and beta-hairpin peptide. *J Phys Chem B* 2004;108:6582–6594.
82. Snow CD, Sorin EJ, Rhee YM, Pande VS. How well can simulation predict protein folding kinetics and thermodynamics? *Annu Rev Biophys Biomol Struct* 2005;34:43–69.
83. Onuchic JN, Luthey-Schulten Z, Wolynes PG. Theory of protein folding: the energy landscape perspective. *Annu Rev Phys Chem* 1997;48:545–600.
84. Steinhauser MO. A molecular dynamics study on universal properties of polymer chains in different solvent qualities. Part 1. A review of linear chain properties. *J Chem Phys* 2005;122:094901.
85. The radius of gyration tensor is defined as follows: For a polypeptide chain comprised of N atoms in a specific conformation let \mathbf{r}_i denote the position vector of the i th atom and \mathbf{r}_{CM} the position vector of the center-of-mass. We first compute N -quantities of the form $\mathbf{s}_i = \mathbf{r}_i - \mathbf{r}_{CM}$ and construct the gyration tensor as a dyadic product using the formula:

$$\mathbf{T} = \frac{1}{N+1} \sum_{i=0}^N (\mathbf{s}_i \otimes \mathbf{s}_i). \quad (5)$$
86. Schäfer L. Excluded volume effects in polymer solutions as explained by the renormalization group. Berlin: Springer; 1999. p 305–343.
87. Metropolis N, Rosenbluth AW, Rosenbluth MN, Teller AH, Teller E. Equation of state calculations by fast computing machines. *J Chem Phys* 1953;21:1087–1092.
88. Rubenstein M, Colby RH. Polymer physics. Oxford: Oxford University Press; 2003. p 97–104.
89. Engh RA, Huber R. Accurate bond and angle parameters for X-ray protein structure refinement. *Acta Cryst* 1991;47:392–400.
90. Allen MP, Tildesley DJ. Computer simulation of liquids. New York: Oxford University Press; 1987. p 185–188.
91. Gentle JE. Elements of computational statistics. New York: Springer-Verlag; 2002. p 69–98.
92. Paci E, Cavalli A, Vendruscolo M, Caffisch A. Analysis of the distributed computing approach applied to the folding a small β peptide. *Proc Natl Acad Sci U S A* 2003;100:8217–8222.
93. Woody RW. Circular dichroism of unordered polypeptides. *Adv Biophys Chem* 1992;2:37–79.
94. Kohn JE, Millett IS, Jacob J, Zagrovic B, Dillon TM, Cingel N, Dothager RS, Seifert S, Thiyagarajan P, Sosnick TR, Hasan MZ, Pande VS, Ruczinski I, Doniach S, Plaxco KW. Random-coil behavior and the dimensions of chemically unfolded proteins. *Proc Natl Acad Sci U S A* 2004;101:12491–12496.
95. Chan HS, Dill KA. Polymer principles in protein structure and stability. *Annu Rev Biophys Biomol Chem* 1991;20:447–490.
96. Lifshitz IM, Grosberg AY, Khokhlov AR. Some problems of the statistical physics of polymer chains with volume interaction. *Rev Mod Phys* 1978;50:684–713.
97. PROSS: Dihedral angle-based secondary structure assignment. 2005. Available at: <http://roselab.jhu.edu/utis/pross/>.
98. Ramirez-Santiago G, Jose JV. Critical exponents of the fully frustrated 2-dimensional xy-model. *Phys Rev B* 1994;49:9567–9582.
99. Lovell SC, Davis IW, Arendall WB, de Bakker PI, Word JM, Prisant MG, Richardson JS, Richardson DC. Structure validation

- by Calpha geometry: phi, psi and Cbeta deviation. *Proteins* 2003;50:437–450.
100. Rucker AL, Pager CT, Campbell MN, Qualls JE, Creamer TP. Host-guest scale of left-handed polyproline II helix formation. *Proteins* 2003;53:68–75.
101. Eberhardt ES, Raines RT. Amide-amide and amide-water hydrogen bonds: implications for protein folding and stability. *J Am Chem Soc* 1994;116:2149–2150.
102. Ramachandran GN, Sasisekharan V. Conformation of polypeptides and proteins. *Adv Protein Chem* 1968;23:283–487.
103. Guo C, Cheung MS, Levine H, Kessler DA. Mechanisms of cooperativity underlying sequence-independent β -sheet formation. *J Chem Phys* 2002;116:4353–4365.
104. Poirier MA, Jiang H, Ross CA. A structure-based analysis of huntingtin mutant polyglutamine aggregation and toxicity: evidence for a compact beta-sheet structure. *Hum Mol Genet* 2005;14:765–774.
105. Hu H, Elstner M, Hermans J. Comparison of a QM/MM force field and molecular mechanics force fields in simulations of alanine and glycine dipeptides (Ace-Ala-Nme and Ace-Gly-Nme) in water in relation to the problem of modeling the unfolded peptide backbone in solution. *Proteins* 2003;50:451–463.
106. Sikorski P, Atkins E. New model for crystalline polyglutamine assemblies and their connection with amyloid fibrils. *Biomacromolecules* 2005;6:425–432.
107. Khare SD, Ding F, Gwanmesia KN, Dokholyan NV. Molecular origin of polyglutamine aggregation in neurodegenerative diseases. *PLoS Comp Biol* 2005;1:0230–0235.
108. Stork M, Giese A, Kretzschmar HA, Tavan P. Molecular dynamics simulations indicate a possible role of parallel beta-helices in seeded aggregation of poly-gln. *Biophys J* 2005;88:2442–2451.
109. Finkelstein AV. Rate of β -structure formation in polypeptides. *Proteins* 1991;9:23–27.
110. Rhee YM, Pande VS. Multiplexed-replica exchange molecular dynamics method for protein folding simulations. *Biophys J* 2003;84:775–786.